International Journal of Mechanical Engineering and Robotics Research

ISSN 2278 – 0149 www.ijmerr.com
Vol. 4, No. 1, January 2015


*Research Paper*

# ANALYSIS OF RZEPPA AND CARDAN JOINTS IN MONORAIL DRIVE TRAIN SYSTEM

Sang June Oh[1]* and John T Woscek[1]

*Corresponding Author: Sang June Oh, ✉sjoh@fullerton.edu

The objective of this paper is to determine the best joint design in the driveshaft of monorail drive train systems. Two of the most common joints used in these types of drive train systems are Rzeppa and Cardan joints. Constant velocity joint such as Rzeppa joint can operate at a much larger joint angle for desired torque transmission than non-constant velocity joints such as Cardan joint. However, constant velocity joints are more expensive to manufacture than more versatile Cardan joints. Therefore, there has been a constant debate in determining which joint type would be optimal. The paper utilizes typical material characteristics and common operating conditions of Rzeppa and Cardan joints. Then, the bending moment couples, which are generated during operation of these joints are analyzed with finite element analysis. This helps in determining the maximum allowable joint angle in using one joint type over the other. The paper further examines the fatigue factor of safety and provides a general guideline in determining the better option between the two. It is determined from these analyses that Rzeppa joint is a better option for general monorail drive train systems. However, Cardan joint may be adequate if the joint angle is very small.

Keywords: Rzeppa joint, Cardan joint, Monorail train, CV joint, Non-CV joint

## INTRODUCTION

Non-Constant Velocity (NCV) joint such as Cardan joint (Universal joint, U-joint, or Hooke joint) and Constant Velocity (CV) joint such as Rzeppa joint are couplings in a driveshaft used to transmit power in various automotive and machinery applications. Both allow parts of a machine not in line with each other limited freedom to move in any direction while transmitting rotary motion (Seherr-Thoss *et al.*, 1998). These two types have their own advantages and disadvantages, as well as their own unique brand of characteristics, which makes them attractive for various applications.Therefore, the intricate workings of both Non-Constant Velocity (NCV) and Constant Velocity (CV) joints will be explored by narrowing the focus to two specific joint

[1] Department of Mechanical Engineering, California State University, Fullerton, Fullerton, CA 92831, US.

types: Rzeppa Joint (CV type) and Cardan Joint (NCV type).

One method of transportation that utilizes both of these joints in its drive system is a straddle-type monorail train (Sekitani *et al.*, 2005). Various early designs of monorail train systems utilized the Rzeppa CV Joint to transmit power with constant velocity as the train moved through various turns and elevations. As time progressed, manufacturers started to develop Cardan NCV joint to replace Rzeppa joint in an effort to save cost. However, due to the nature of NCV joints, questions have arisen as to how reliable of a replacement the Cardan Joint can be. Monorail manufacturers have stated that as long as the angle of operation is not too high, the Cardan Joint will be adequate. For a long period of time, manufacturers generally indicate Cardan joints should be restricted to angles of 15 degrees or less (Carmichael, 1950). However, this threshold angle is difficult to pinpoint, since the operating angles for different monorail train systems are not the same. Therefore, one of the objectives of this paper is to provide a general guideline and determine the threshold angle based on the design of both joints and further justify whether or not Cardan joints can be an adequate replacement for Rzeppa joints.

Rzeppa Joint is defined as a self-supported constant velocity joint that contains an outer and inner race, connected through balls positioned in the constant velocity plane by axially offset curved grooves. The balls are maintained in this plane by a cage located between the two races (Wagner and Cooney, 1991). There are multiple configurations that fit this definition, each of which yield various

Figure 1A: Cross Sectional View of Bell-Type Rzeppa Joint

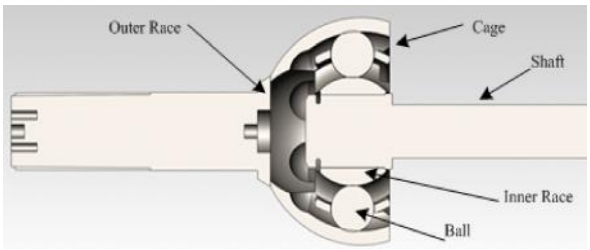


Figure 1B: Dissected View of Bell-Type Rzeppa Joint

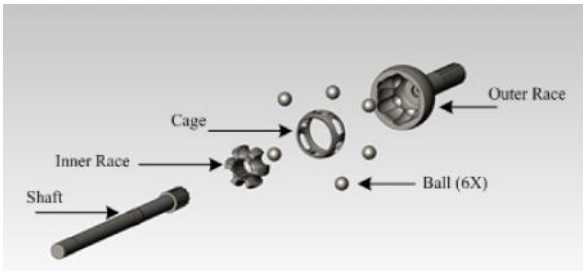


characteristics. This paper will be focusing on the bell-type Rzeppa Joint, illustrated in Figures 1A and 1B.

The bell-type Rzeppa Joint is primarily used in applications where a drive torque is required, such as on the drive shaft of a car or in this case, the drive shaft of a monorail. Further observation of Figures 1A and 1B show how the outer race contains a set of splines, which will mate with a drive flange that is mounted to a drive wheel. The inner race of the Rzeppa Joint is also splined, and this race mates with the external splines on a drive shaft that is held in place by a snap (or retaining) ring, as seen in Figures 1A and 1B. The balls that ride within the six grooves are made of pure steel. For the joint used in this study, the balls each have an overall diameter of 1.6870 inches. Rzeppa joint design has many appealing advantages (Qin *et al.*, 2003). One

of these is its ability to transmit constant velocity at a relatively high angle, close to 45 degrees, and some as high as 51 degrees. Also, because of its rugged and compact design, it allows for a relatively high torque capacity for a given swing diameter. This robust design also allows for it to withstand high external axial forces of an intermittent nature (Wagner and Cooney, 1991). However, the robust design of the Rzeppa Joint leads to some major disadvantages as well. Since it is sturdy and heavy, the Rzeppa Joint is very expensive to manufacture, not only in material cost but also in machining as well. Since these joints need to be either forged or casted, it is very difficult to hold some of the demanding tolerances needed for various features, such as the grooves for the balls and the spherical diameters of the cage and inner race. The Rzeppa Joint is typically made of a low to medium carbon steel. For the analysis of this paper, the chosen material is AISI 4130, taken from ASTM standard A322 for standard grade Hot-Wrought Steel Bar stock (ASTM, 2004).

The Cardan Joint is one of the most common non-constant velocity joints used in the automotive and power transmission industries. The SAE Driveshaft and Universal Joint Design Guide defines Cardan Joint as a nonconstant velocity joint consisting of two yokes drivably connected by a cross through four bearings (Wagner and Cooney, 1991). In general, it is simple to manufacture a Cardan Joint for use in any application. This allows for a greater flexibility in the design of the slip and tube yokes, ultimately yielding many different styles that will perform the same function. One of a very commonly used Cardan joint, "wing-bearing type" Cardan Joint will be chosen for this paper. The "wing-bearing type" Cardan Joint utilizes a slip yoke and tube yoke and an illustration of the entire assembly is shown in Figures 2A and 2B.

Figure 2A: Cross Sectional View of "Wing-Bearing Type" Cardan Joint

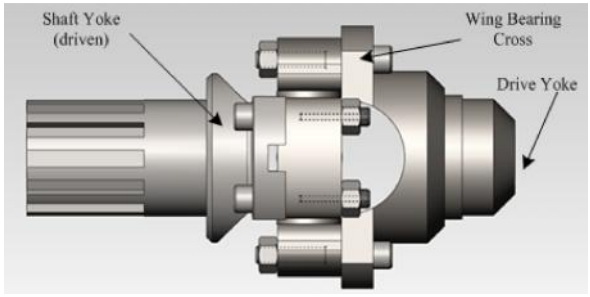


Figure 2B: Dissected View of "Wing-Bearing Type" Cardan Joint

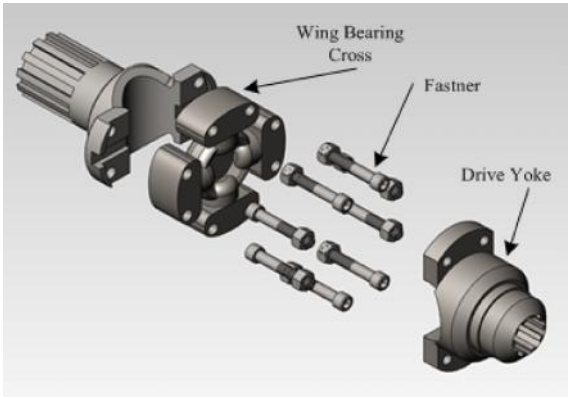


Primarily, these "wing bearing" types of Cardan Joints are used on automotive drive shafts and other applications. This particular style is attractive simply because of the ease of attachment; rather than using a pin to connect the yokes to the cross, fasteners are used to mate the yoke to the cross at the proper attachment points. The drive yoke is allowed to articulate independent of the shaft yoke due to the roller bearings located within the cross. Typically, the driven yoke is splined in order to mate with the other end of the drive shaft.

One of the biggest advantages of Cardan Joint is simplicity in manufacturability regardless of its size. This allows for use in a wide variety of applications ranging from small machinery to large trucks. In addition to its ease of manufacturability, this design also yields a longer durability and minimum maintenance since there are less rotating parts than Rzeppa Joint, thereby minimizing many points of failure. One of the disadvantages of this joint type is that it does not transmit the same output velocity at higher joint angles. This can certainly pose an issue for a monorail train drive system. This is why it is imperative that the threshold angle be determined in order to validate the use of the Cardan Joint in what would be a constant velocity application.

For this paper, the components of Cardan joints were chosen that can easily be obtained through manufacturers. The drive yoke is a Neapco Wing Bearing End Yoke 7C Series, part number 10508J. The Shaft Yoke is a Neapco Wing Bearing Yoke Shaft 7C Series, part number 5505J. The Universal Joint Cross is a Neapco/Spicer Wing Bearing Universal Joint 7C Series, part number 5-7105X. These parts were all chosen for the analysis because this particular driveshaft (7C) is a commonly used one in heavy trucks and machinery. These parts are typically made from a low to medium carbon steel.

Since the Rzeppa Joint is being analyzed as AISI 4130, the Cardan Joint will also be assumed to be this same material for comparison purpose in the analysis. Basically, the Cardan Joint boils down to a simple design with complex characteristics (as opposed to Rzeppa joint being complex design with simple characteristics). However, it is important to understand the input and output torque ratio to predict the amount of stress that will be seen by the yokes, and ultimately determine the life cycle of a Cardan Joint. This will help in determining whether or not the Cardan Joint would be an adequate replacement for the Rzeppa Joint.

## MATERIALS AND METHODS

The Rzeppa Joint and the Cardan Joint are both designed to operate at a maximum angle of 45°. As previously mentioned, the Rzeppa Joint will yield constant velocity across all of these angles, whereas the Cardan Joint will not. Besides the obvious geometric design differences in both joints, the Rzeppa and Cardan Joints yield a pair of torques on both couplings during angular navigation called “Secondary Bending Moment Couples”, which mathematically explain the forces exerted on these joints while transmitting torque at various angles (Wagner and Cooney, 1991).

The Rzeppa Joint’s bending moment couples at different angles are given by the following equation:

$$C = C_1 = T \tan\frac{\bar{}}{2} \quad \text{...(1)}$$

where $C$ is the secondary couple on the driving member, $C_1$ is the secondary couple on the driven member, $T$ is the input torque and $\bar{}$ is the angle between joints, also known as the joint angle.

The Cardan Joint’s bending moment couples are a bit more complex. Due to its nature, the bending moments of the driving yoke and driven yoke will depend on different situations during motion. The driving yoke’s bending moment couples are given by the following equation:

$$C = T \tan^{-} \cos \quad ...(2)$$

For the driven yoke, the bending moment couple is given by the following equation:

$$C_1 = T \sin^{-} \sin \quad ...(3)$$

where $C$ is the secondary couple on the driving member, $T$ is the input torque, $^{-}$ is the joint angle, and is the angle of rotation of the driving yoke from a position where it is normal to the joint angle plane. Please note that the orientation of the joint angle $^{-}$ and the angle normal to it is . The driving yoke can articulate both horizontally and vertically, which yields these two different angles. In order to justify the validity, the comparison study will be performed with = 45 degrees in the Cardan Joint. This was chosen to see how effective Cardan Joint can be, under worst circumstances, in comparison to Rzeppa Joint.

Another factor in this design consideration is the fatigue life. In many industries, the easiest method of explaining fatigue life is through the Fatigue Factor of Safety (FOS). This FOS is based on the "stress-life" (Budynas and Nisbett, 2011). One of the factors in determining this FOS is the Corrected Endurance Limit, $S_e$, which takes into effect all surface finishing, temperature and shape, and is given by the following equation (Budynas and Nisbett, 2011):

$$S'_e k_a k_b k_c k_d k_e k_f = S_e \quad ...(4)$$

where $S'_e$ is the Mean Endurance Limit of the parent material, $k_a$ is the reduction of the material strength due to Surface Finish, $k_b$ is the size effect, $k_c$ is the Loading Factor, $k_d$ is the temperature factor, $k_e$ is the reliability factor, and $k_f$ is the stress concentration factor. This Corrected Endurance Limit is then divided by the Goodman Equivalent Stress to find the FOS (Budynas and Nisbett, 2011). The Goodman Equivalent Stress is found by the following equation:

$$\pm_{eq} = \pm_{amp} + \left( \pm_{mean} * \frac{S_e}{\pm_{uts}} \right) \quad ...(5)$$

where $\pm_{amp}$ is the amplitude stress, $\pm_{mean}$ is the average, or mean stress, $S_e$ is the Corrected Endurance Limit, and $\pm_{uts}$ is the Ultimate Tensile Strength of the parent material. Dividing Equation (4) by Equation (5) yields the Fatigue Factor of Safety in Equation (6) below:

$$FOS = \frac{S_e}{\pm_{eq}} \quad ...(6)$$

Ultimately, the goal is to determine whether or not a simple joint design can replace a complex one. From further observation of Equations (2 and 3), an important mathematical assumption can be made. The effort of the industry in attempting to replace Rzeppa CV Joints with more economical Cardan Joint is debatable. If the guideline for the use of these joints can be found, it can be used as a benchmark for design considerations for all transportation drive assemblies.

## RESULTS AND DISCUSSION

Equations (1)-(3) were used for calculating the Secondary Bending Moment Couples for each joint. Table 1 below outlines the assumed operating conditions of the theoretical Monorail train, with shaft torques at startup, acceleration and cruising speeds, along with the assumed operating times for one year.

Table 2 below shows the results from calculating the bending moment couples for

| Table 1: Operating Conditions of Theoretical Monorail | | | | |
|---|---|---|---|---|
| **Description** | **Frequency (% of Total Operation)** | **Shaft Torque (*ft-lb*)** | **Shaft Torque (*in-lb*)** | **Shaft Velocity (rpm)** |
| Startup | 9% | 2500 | 30000 | 150 |
| Acceleration | 4% | 1300 | 15600 | 210 |
| Cruise | 87% | 840 | 10080 | 250 |
| Assumed hours per day | | 13.70 | | |
| Assumed days per year | | 365 | | |
| Assumed hours per year | | 5000 | | |

each joint with Equations (1)-(3) for the startup shaft torque. The joint angles in the first column in this and the subsequent tables pertaining to Bending Moment Couples were chosen to show the small angle approximation mentioned in the previous section, and to outline a

| Table 2: Bending Moment Couples at Startup Stage | | | |
|---|---|---|---|
| **Description** | **Bending Moment Couples Cardan Joint, = 45°** | | **Bending Moment Couples Rzeppa Joint** |
| **Joint Angle ¯ (°)** | ***C* (Driving Yoke), *in-lb*** | **$C_1$ (Driven Yoke), *in-lb*** | **$C = C_1$, *in-lb*** |
| 1 | 370.28 | 370.22 | 261.81 |
| 2 | 740.78 | 740.33 | 523.65 |
| 3 | 1111.74 | 1110.21 | 785.58 |
| 4 | 1483.37 | 1479.76 | 1047.62 |
| 5 | 1855.91 | 1848.85 | 1309.83 |
| 6 | 2229.60 | 2217.38 | 1572.23 |
| 12 | 4509.01 | 4410.47 | 3153.13 |
| 15 | 5684.06 | 5490.38 | 3949.57 |
| 45 | 21213.20 | 15000.00 | 12426.41 |

| Table 3: Bending Moment Couples at Acceleration Stage | | | |
|---|---|---|---|
| **Description** | **Bending Moment Couples Cardan Joint, = 45°** | | **Bending Moment Couples Rzeppa Joint** |
| **Joint Angle ¯ (°)** | ***C* (Driving Yoke), *in-lb*** | **$C_1$ (Driven Yoke), *in-lb*** | **$C = C_1$, *in-lb*** |
| 1 | 192.54 | 192.52 | 136.14 |
| 2 | 385.21 | 384.97 | 272.30 |
| 3 | 578.10 | 577.31 | 408.50 |
| 4 | 771.35 | 769.47 | 544.76 |
| 5 | 965.08 | 961.40 | 681.11 |
| 6 | 1159.39 | 1153.04 | 817.56 |
| 12 | 2344.68 | 2293.45 | 1639.63 |
| 15 | 2955.71 | 2855.00 | 2053.78 |
| 45 | 11030.87 | 7800.00 | 6461.73 |

| Table 4: Bending Moment Couples at Cruise Stage | | | |
|---|---|---|---|
| **Description** | **Bending Moment Couples Cardan Joint, = 45°** | | **Bending Moment Couples Rzeppa Joint** |
| **Joint Angle ¯ (°)** | ***C* (Driving Yoke), *in-lb*** | **$C_1$ (Driven Yoke), *in-lb*** | **$C = C_1$, *in-lb*** |
| 1 | 124.41 | 124.39 | 87.97 |
| 2 | 248.90 | 248.75 | 175.95 |
| 3 | 373.54 | 373.03 | 263.95 |
| 4 | 498.41 | 497.20 | 352.00 |
| 5 | 623.59 | 621.21 | 440.10 |
| 6 | 749.14 | 745.04 | 528.27 |
| 12 | 1515.03 | 1481.92 | 1059.45 |
| 15 | 1909.84 | 1844.77 | 1327.06 |
| 45 | 7127.64 | 5040.00 | 4175.27 |

perspective of how both joints react across the spectrum of various operating angles. 12° is also shown in this table because this is the value at which tan¯ and sin¯ really begin to separate in value and the small angle approximation is no longer valid. However, this does not mean that 12° is the "threshold angle" for the two joints. Tables 3 and 4 show the results from calculating the bending moment couples for each joint from Equations (1)-(3) using the acceleration phase and cruise stages.

The values from these tables were used as torques in a Finite Element Analysis (FEA) of both joints to ultimately determine the stresses in each joint and where certain failure points were expected. The FEA model of the Rzeppa Joint is shown below in Figure 3, and the values for the peak stress are given in Table 5 for operating angles of +/-1°, +/–6° and +/–12°. These values were chosen because they are the most common operating angles for this application and they yield a broad spectrum of the various stresses seen by these two joint designs.

Figure 3: FEA Model of Rzeppa Joint

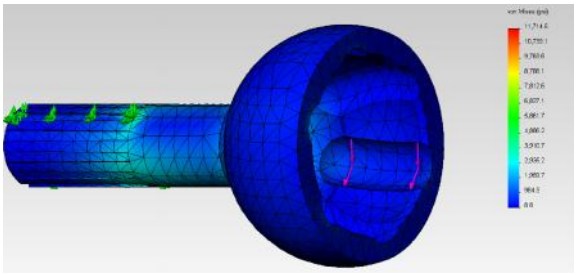

| Table 5: Rzeppa Joint FEA | | |
|---|---|---|
| Startup Stage Torque | | Stress (psi) |
| | Max Stress at 1° | 961 |
| | Max Stress at 6° | 4632 |
| | Max Stress at 12° | 10015 |
| Acceleration Stage Torque | | |
| | Max Stress at 1° | 600 |
| | Max Stress at 6° | 2407 |
| | Max Stress at 12° | 4830 |
| Cruise Stage Torque | | |
| | Max Stress at 1° | 256 |
| | Max Stress at 6° | 1556 |
| | Max Stress at 12° | 3120 |

The outer race of the Rzeppa Joint was the only part that was analyzed since the largest stress occur in this area during motion. The

splines on the outer shaft were fixed, which is intended to represent the load wheel at a dead stop. The input torque was applied to the inner surfaces of the Rzeppa joint, and the value of this input torque is the bending moment couple calculated from Equation (1). The bending moment couple was used since it is dependent on the operating angle and the initial drive torque from the motor. The maximum stress is seen at the top of the splines (the faint green area in Figure 3).

The FEA model of the Cardan Joint is shown below in Figure 4, and the peak stress values are given in Table 6.

Figure 4: FEA Model of the Cardan Joint

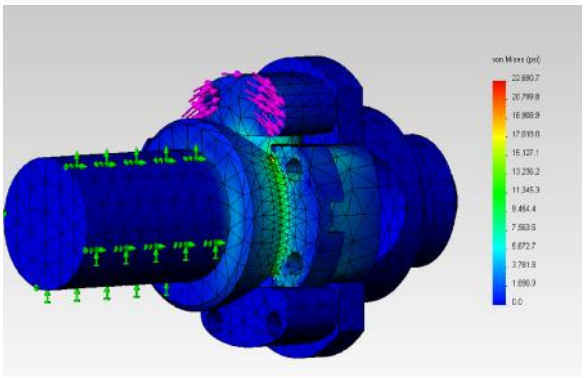

Table 6: Cardan Joint FEA, = 45°

| Startup Stage Torque | | Stress (psi) |
|---|---|---|
| | Max Stress at 1° | 1814 |
| | Max Stress at 6° | 10933 |
| | Max Stress at 12° | 22131 |
| Acceleration Stage Torque | | |
| | Max Stress at 1° | 941 |
| | Max Stress at 6° | 5683 |
| | Max Stress at 12° | 11498 |
| Cruise Stage Torque | | |
| | Max Stress at 1° | 694 |
| | Max Stress at 6° | 4197 |
| | Max Stress at 12° | 8491 |

The Cardan Joint was analyzed as a whole, with the splines on the yoke shaft suppressed for easier meshing. From observation of Figure 4, the “splines” on the yoke shaft, or driven yoke, are fixed (simulating the load wheel at dead stop) and the input torque (Cardan Joint Bending Moment Couple values from Tables 2-4) is applied to the wing bearings on the appropriate sides. The driving torque is applied from the driving yoke, moving counterclockwise, and the driven torque is applied to the driven yoke, moving clockwise. The maximum stress is seen in the joining radius of the driven yoke (faint green area in Figure 4).

The stress values from Tables 5 and 6 were placed in a fatigue calculator to determine the Factor of Safety using a Reliability Factor ($k_e$) of 94.95% (Assumed factor for General Use and Reliability Critical Parts). The Fatigue Factor of Safety was calculated using Equations (4)-(6) discussed in the Introduction. The Fatigue Factors of Safety for both joints at each operating condition are shown in

Table 7: Fatigue Factors of Safety for Both Joints

| | | Rzeppa Joint FOS | Cardan Joint FOS |
|---|---|---|---|
| Startup Stage Torque | | | |
| | Max Stress at 1° | 25.04 | 13.24 |
| | Max Stress at 6° | 3.66 | 2.19 |
| | Max Stress at 12° | 1.99 | 1.78 |
| Acceleration Stage Torque | | | |
| | Max Stress at 1° | 45.02 | 27.2 |
| | Max Stress at 6° | 7.49 | 4.51 |
| | Max Stress at 12° | 3.98 | 2.09 |
| Cruise Stage Torque | | | |
| | Max Stress at 1° | 70.65 | 42.28 |
| | Max Stress at 6° | 13.03 | 7.03 |
| | Max Stress at 12° | 5.78 | 3.48 |

Figure 5A: Rzeppa Joint Stresses versus Angle at Startup

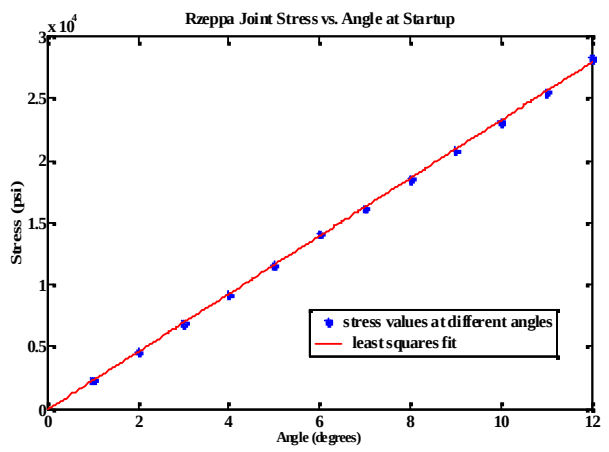


Figure 5B: Cardan Joint Stresses versus Angle at Startup

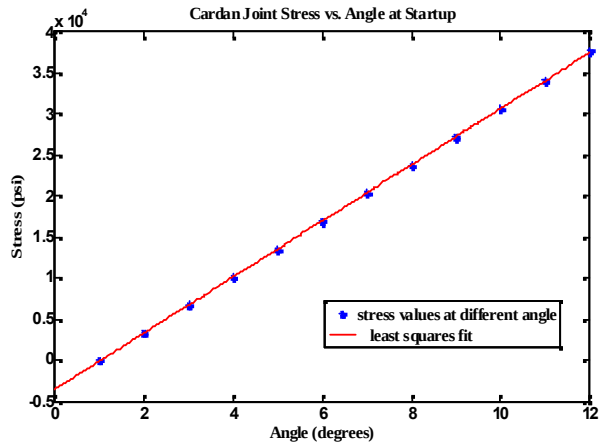


Table 7. The goal of the fatigue calculator is to keep the FOS above a value of 1 to maintain infinite life.

The following two figures show the stress distributions for both joints across all angles from 1°-12° for the startup stage.

Figures 5A and 5B show that the stresses for both joints increase linearly as the bending moment couples increase, and the only difference being the actual values of the stresses between the two joints. The stress figures for acceleration and cruise stages have been omitted here because the linear trend is the same as the startup stage. Both the Rzeppa Joint and Cardan Joint exhibit increasing stresses as operating angle increases. This is due to the direct proportionality of the joint angle and the bending moment couple (from observation of Equations (1)-(3). The small angle approximation (tan ¯ ≈ sin ¯) mentioned in the introduction section is also quite valid up to about 12°, however the bending moment couples on the Cardan Joint begin to deviate well before this stage.This in turn yields higher stresses on the both the driven and driving yokes of the Cardan Joint.

From observation from Table 2, it is apparent that the bending moments on the Rzeppa Joint are close to half the magnitude of the Cardan Joint. This hints to a theory that the Rzeppa Joint's stresses would be half as much as the Cardan Joint's. This is a valid prediction since Equation (1) for the Rzeppa Joint's bending moment contains a ¯/2 term in the calculation, whereas Equations (2) and (3) for the Cardan Joint only contain a ¯ term. However, the analysis shows that the Cardan Joint yields astress that is slightly lower than the Rzeppa at a 1° operating angle for startup, even though the bending moment couples are higher (for the case of = 0, however).

At higher angles, the values of the bending moment couples on the Cardan Joint deviate from each other, as mentioned before. This yields higher stresses on the Cardan Joint, about 3,000 psi greater than the Rzeppa Joint. Ultimately this also constitutes a lower factor of safety as the operating angle increases, as seen in Table 7. While both will achieve infinite life according to the calculator, it is safer to go with the Rzeppa joint rather than the Cardan

Joint especially if the operating angles are going to be higher than 12°.

It is also important to reiterate the fact that all of the analysis of the Cardan Joint has been set in one dimension; that is, , the angle normal to the plane of the joint angle, has been set to 45 degrees (the worst possible case scenario). This is another reason why it is important to understand the application and the environment that these joints will be used in and take into account all possible outcomes.

One possible alternative to this issue could be to use the Double Cardan Joint, which utilizes two Cardan Joints coupled in the center, which eliminate the lopsided bending moment couples on the driven and driving sides (Fischer and Paul, 1991; and Biancolini *et al.*, 2003). The only issue with using this joint in this particular application is the size; having two Cardan Joints coupled at the center will protrude much further than desired, thus requiring two smaller Cardan Joints which may not be strong enough to transmit the drive torques. Another possible alternative is the Thompson Coupling CV Joint, which tries to blend the best of both the Rzeppa and Cardan Joints into one unit (Lin and Liao, 2007). This definitely could be a solution, but this joint will need to be tested a lot more in order to validate its use in this application as it has not been used in a Monorail train yet.

## CONCLUSION

The most important point to make from this study is that if the joint angle ¯ low, say approximately well within –6° and +6°, and if the angle is minimal (near zero), the Cardan Joint can be adequate. However, if at any point in motion the operating angle exceeds 6° in any direction, the Rzeppa Joint will be the better option in terms of fatigue and reliability. Therefore, the "threshold angle" can be said to be approximately 6° in either direction of angle. Exploring the differences between Constant and Non-Constant Velocity Joints reveals that choosing between the two is not an easy decision. However, it can be concluded unless the operating angle is very low, Rzeppa Joint should be choice in most straddle type monorail driving operation to have more robust operation without any troubling issues.

## REFERENCES

1. ASTM International & American Society for Testing & Materials (2004), Annual Book of ASTM Standards, American Society for Testing & Materials.
2. Biancolini M E, Brutti C, Pennestrì E and Valentini P P (2003), "Dynamic, Mechanical Efficiency, and Fatigue Analysis of the Double Cardan Homokinetic Joint", *International Journal of Vehicle Design*, Vol. 32, No. 3, pp. 231-249.
3. Budynas R G and Nisbett J K (2011), *Shigley's Mechanical Engineering Design*.
4. Carmichael C (1950), *Kent's Mechanical Engineers' Handbook*.
5. Fischer I S and Paul R N (1991), "Kinematic Displacement Analysis of a Double-Cardan-Joint Driveline", *Journal of Mechanical Design*, Vol. 113, No. 3, pp. 263-271.
6. Lin C C and Liao W K (2007), "The Displacement Analysis of a Concentric

Double Universal Joint", In 12th IF to MM World Congress on Mechanism and Machine Science, Comité Franáais pour la Promotion de la Science des Mecanismes et des Machines Besanáon, France.

7. Qin G, Zhang Y Q and Wu C L (2003), "Dynamics Simulation Analysis System for Ball Basket Constant Velocity Universal Joint".
8. Seherr-Thoss H C, Schmelz F and Aucktor E (1998), *Universal Joints and Driveshafts*, Beijing Institute of Technology Press, Beijing.
9. Sekitani T, Hiraishi M, Yamasaki S and Tamotsu T (2005), "China's First Urban Monorail System in Chongqing", *Hitachi Review*, Vol. 54, No. 4, p. 193.
10. Wagner E R and Cooney C E (1991), "Universal Joint and Driveshaft Design Manual", Society of Automotive Engineers, Warrendale, PA.